CHALMERS
UNIVERSITY OF TECHNOLOGY

Dual-Band Filtering Slot Array Antenna for W-Band Application

Citation for the original published paper (version of record):
Fang, M., Santiago, D., Yang, J. et al (2026). Dual-Band Filtering Slot Array Antenna for W-Band Application. IEEE Transactions on Antennas and Propagation, 74(1): 434-444.
http://dx.doi.org/10.1109/TAP.2025.3617124

(article starts on next page)

Dual-Band Filtering Slot Array Antenna for W-Band Application

Mu Fang, David Santiago, Jian Yang, *Senior Member, IEEE*, Ivan Arregui, *Member, IEEE*, Miguel A. G. Laso, *Fellow, IEEE*, Thomas Emanuelsson, Ashraf Uz Zaman, *Senior Member, IEEE*, and Ahmed A. Kishk, *Life Fellow, IEEE*

***Abstract*—A co-aperture dual-band linearly polarized slot array based on ridge gap waveguide (RGW), operating at the 74–78- and 102–106-GHz bands, is designed. In each subarray, two groups of longitudinal slots for two frequency bands are excited by a single RGW channel to achieve dual-band unidirectional radiation. Additionally, grooves and notches are implemented inside the RGW structure to improve dual-band matching, and two bandpass filters (BPFs) are incorporated at each side of the subarray to realize independent dual-band feeding while also providing filtering characteristics. The proposed subarray operates as a single channel. It can expand into a multichannel array, enabling multiple-input multiple-output (MIMO) when each subarray is individually excited or broadside radiation when all subarrays are simultaneously excited. A planar array of four subarray columns was fabricated to validate the dual-band concept and its broadside radiation performance. The simulated and measured results show good agreement.**

***Index Terms*—Bandpass filter (BPF), dual bands, gap waveguide (GWG), slot array.**

I. Introduction

WAVEGUIDE slot array antennas have extensive use in wireless communication and radar systems, attributed to their low loss, high mechanical strength, and substantial power-handling capabilities [1], [2]. Their most common applications include generating high-gain beams [3], enabling multiple-input multiple-output (MIMO) capabilities [4], and performing beam scanning [5], typically realized within a single frequency band. It is also appealing to achieve dual-band radiation with slot arrays, as it enhances system flexibility and functionality within a relatively compact size. Various dual-band slot array designs have been reported [6], [7], [8], [9], [10], [11], [12], [13], [14], [15], [16], [17], [18], [19], [20], [21], [22], [23], [24].

In [6], a dual-band coaxial resonant cavity structure is proposed, enabling a single slot to achieve dual-band single-polarized radiation. A corporate network feeds these cavities to realize a planar array. In [7], multiple dual-band dual-polarized slots are excited by a single high-order mode cavity resonator, eliminating the need for a power-splitting network. However, both designs differ from series-fed waveguide slot arrays and can only support broadside radiation.

A more common dual-band configuration employs multiple closely packed waveguide slot arrays [8], [9], [10], [11], [12], [13], [14], [15], [16], [17], [18], which enables broadside radiation and supports independent channel operation. In [8], [9], [10], [11], [12], [13], and [14], offset broad-wall longitudinal slot arrays and narrow-wall slot arrays are interlaced to realize a dual-polarized array, where the two sets of arrays can operate either at different bands or the same band due to independent channels. It is worth noting that those feeding waveguides are typically loaded with a ridge to reduce the element spacing, and the side-wall slots must extend into the neighboring walls of the feeding waveguide, which results in a complex nonplanar structure. In [15], [16], [17], and [18], broad-wall longitudinal slot arrays are employed for both bands to enable dual-band single-polarized radiation. In this setup, the high-frequency (HF) slot arrays are interleaved and stacked above the low-frequency (LF) ones to minimize further the element spacing, which leads to a multilayer structure. Although those designs can achieve the desired performance, the densely arranged waveguide channels, nonplanar apertures, and complex 3-D structures can significantly increase the manufacturing complexity and cost, particularly at high millimeter-wave frequencies.

In addition, several attempts have been reported to excite dual-band slots with a single waveguide channel [19], [20], [21], [22], [23], [24], aiming to achieve dual-band radiation in a simpler structure while maintaining the flexibility of independent channel operation. In [19] and [20], two sets of slots for dual bands are located on opposite broad walls of the waveguide. However, this configuration only radiates in opposite directions. In [21], [22], and [23], dual-band longitudinal slots are etched on the same broad wall of a waveguide but in different regions along the longitudinal direction, which

Received 28 March 2025; revised 28 August 2025; accepted 23 September 2025. Date of publication 8 October 2025; date of current version 21 January 2026. This work was supported in part by Swedish Innovation Agency Grant through the Eureka CELTIC Framework under Grant 2020-02889 and in part by Spanish Ministerio de Ciencia e Innovación—Agencia Estatal de Investigación through MCIN/AEI/10.13039/501100011033 under Project PID2020-112545RB-C53. *(Corresponding author: Mu Fang.)*

Mu Fang, Jian Yang, and Ashraf Uz Zaman are with the Department of Electrical Engineering, Chalmers University of Technology, 412 96 Gothenburg, Sweden (e-mail: mu.fang@chalmers.se; jian.yang@chalmers.se; zaman@chalmers.se).

David Santiago, Ivan Arregui, and Miguel A. G. Laso are with the Institute of Smart Cities (ISC), Department of Electrical, Electronic, and Communications Engineering, Public University of Navarre (UPNA), Campus Arrosadia, 31006 Pamplona, Spain (e-mail: david.santiago@unavarra.es).

Thomas Emanuelsson is with Ericsson AB, 417 56 Gothenburg, Sweden.

Ahmed A. Kishk is with the Department of Electrical and Computer Engineering, Concordia University, Montreal, QC H3G 2W1, Canada.

Digital Object Identifier 10.1109/TAP.2025.3617124

does not create a true co-aperture. In [24], longitudinal and transverse slots are implemented on the same broad wall of a waveguide. However, this design is not a conventional series slot array, as the waveguide is excited by a corporate power divider at the back, resulting in a bulky structure. Moreover, most of these designs exhibit undesired impedance matching and narrow bandwidth, indicating the significant challenge associated with this single waveguide feeding configuration.

Here, we present a W-band dual-band single-polarized filtering slot array based on ridge gap waveguide (RGW), with the main novelties summarized as follows. This design features a shared waveguide channel for dual-band slots, unidirectional radiation, and a truly shared planar aperture, and its configuration is carefully refined to simultaneously support dual-band broadside radiation and independent channel operation (e.g., MIMO) when extending the subarray into a planar array. To the best of authors' knowledge, our proposed design is the first to achieve these functionalities. Additionally, two bandpass filters (BPFs) are incorporated at each side of the subarray to achieve independent dual-band feeding and filtering characteristics. In this unique approach, a dual-band standing-wave slot array is realized through complete reflection provided by two BPFs, distinguishing it from traditional designs that rely on short-circuit terminations. Furthermore, the proposed configuration naturally enables easy integration of RF electronics with the antenna array, offering an alternative to complex diplexers for dual-band excitation and providing greater flexibility in system integration.

The dual bands are 74–78 and 102–106 GHz (frequency ratio = 1.37:1), aiming to facilitate potential applications for 6G wireless networks [25]. In each waveguide channel, HF slots are placed along the inner region of the broad wall, with LF slots arranged on the outer sides of the HF slots. Matching grooves and notches are implemented to improve the dual-band reflection coefficient. The proposed antenna array features a straightforward fabrication process, benefiting from its planar geometry and GWG architecture. By eliminating the need for electrical contact between metal layers [26], [27], [28], [29], [30], GWG greatly simplifies the implementation of antenna arrays at W-band and beyond [31], [32], [33], [34].

This article is organized as follows. Section II explains the mechanism of the dual-band subarray, including the coexistence design of dual-band slots and impedance matching techniques. Section III presents the designs of subarray with independent dual-band feeding enabled by BPFs. Section IV examines a four-column planar array operating in two scenarios: MIMO when each subarray is individually excited (e.g., MIMO radar) and broadside radiation when all subarrays are simultaneously excited. A prototype for broadside radiation is manufactured and measured to verify the concept. The conclusion is provided in Section V.

II. Dual-Band Slot Subarray Design

As shown in Fig. 1, the dual-band subarray design begins with a single-port version. One feeding port is at one side of the waveguide channel for both bands, while the other side of the RGW is short-circuited by connecting the ridge and the top plate, which enables the subarray to operate as

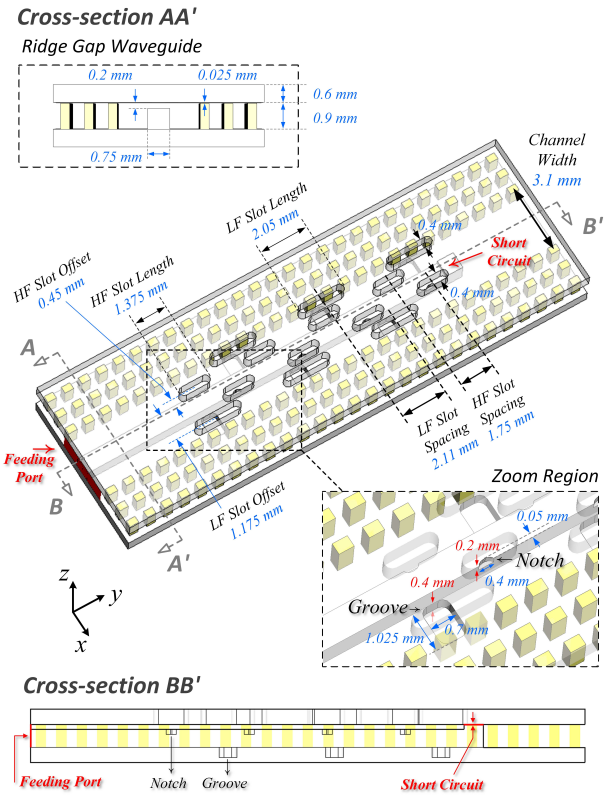

Fig. 1. Structure of the basic dual-band subarray.

a standing-wave slot array antenna at both bands (this short-circuit structure is used solely for simulation purposes). In this design, eight HF slots, operating at 102–106 GHz, are interleaved above the ridge edges, while six LF slots, operating at 74–78 GHz, are positioned in the outer region of the RGW, relatively farther from the ridge. This arrangement positively correlates the offset with the frequency, avoiding overly large spacing between the interleaved HF slots. Furthermore, matching notches are carved on the ridge edges beneath each HF slot, and matching grooves are placed at the bottom of the RGW under each LF slot. The dual-band subarray's operating principle and matching techniques are explained in Sections II-A–II-C.

A. Coexistence of Dual-Band Slots

Given the 1:1.37 frequency ratio, interference between dual-band slots is insignificant. At LF, HF slots are essentially cut off, contributing negligible radiation. At HF, LF slots radiation is significantly suppressed but can slightly radiate in the fundamental mode, while the second-order split-beam mode (resonating at double LF) is not excited. In addition, the ridge primarily influences HF slots, enhancing flexibility in dual-band control, especially with matching structures (notches and grooves). Notably, this configuration potentially supports a broader frequency ratio range (approximately 1:1.2–1:1.85), which will be discussed in future work.

As mentioned, there are still some interactions between the dual-band slots. To evaluate this, the subarray without matching grooves or notches is examined first. The LF performance is initially compared in two scenarios: one with

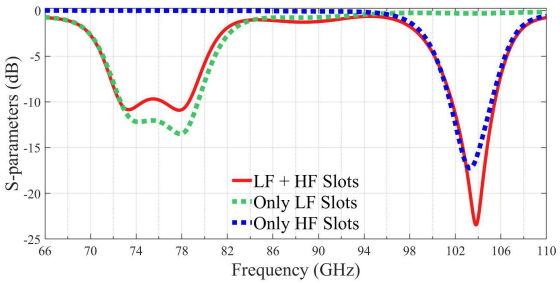

Fig. 2. Comparison of simulated S_{11} of subarrays (without matching techniques) in different cases.

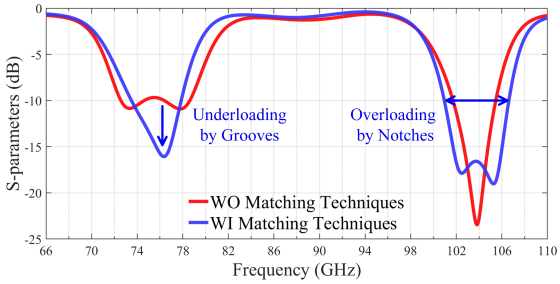

Fig. 3. Simulated S_{11} of dual-band subarrays with and without matching techniques (the curve "without matching techniques" in this figure is the same as the curve "LF + HF slots" in Fig. 2).

both LF and HF slots and the other with only LF slots. As depicted in Fig. 2, with only LF slots, S_{11} is below −12 dB from 74 to 78 GHz, where a noticeable double resonance can be observed, indicating that the LF slots are overloaded. Overload refers to the condition where the total normalized conductance of all slots exceeds unity at the center frequency, causing a slight mismatch but leading to a broader bandwidth [3]. The relatively large offsets of LF slots, necessary for accommodating HF slots, contribute to this high conductance. Although this performance is acceptable, S_{11} deteriorates from −12 dB to around −10 dB upon the addition of HF slots. This resembles an intensified overload effect, despite the bandwidth not further widening.

Similarly, the HF performance is compared with and without LF slots. As depicted in Fig. 2, with only HF slots, S_{11} exhibits a single deep resonance at around 103 GHz with around 3.7-GHz, −10-dB bandwidth, indicating good matching (underload) due to smaller slot offsets [3]. Upon the implementation of LF slots (the HF slot length is slightly tuned), almost identical bandwidth can be achieved.

Hence, it can be concluded that this subarray exhibits excessive overloading at the LF band (double resonance, wider bandwidth, and relatively high reflection level) and underloading at the HF band (single deep resonance and narrower bandwidth). This performance is attributed to the constraints of slot offsets imposed by the coexistence of dual-band slots, and there is very limited space to adjust, especially considering the manufacturing challenges at W-band. Therefore, we propose two alternative matching techniques, grooves and notches, to improve the dual-band reflection coefficient without altering the slot layout.

B. Matching Grooves and Notches

To achieve a lower S_{11} level at the LF band, grooves are placed underneath each LF slot to alleviate their overloading. These grooves act as local vertical extensions of the RGW structure in the regions, where the LF slots are located above, equivalently reducing the relative offset of the LF slots. Fig. 3 illustrates the comparison of the reflection coefficient with and without grooves: the S_{11} is improved from −10 dB to around −15 dB near the center frequency of the LF band (76 GHz) despite a slight reduction in bandwidth. This reduction can be traded off by the depth and length of the groove and further optimized in the subsequent design (together with the LF BPF).

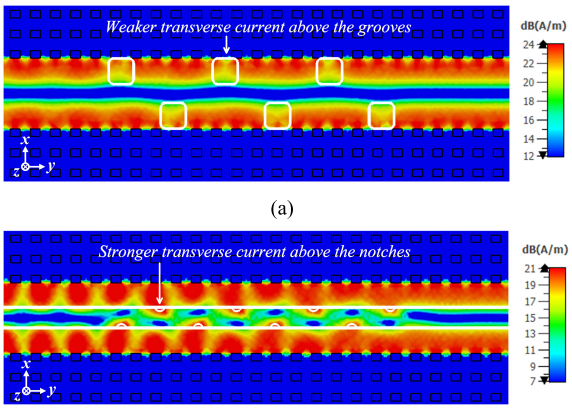

Fig. 4. Surface electric current distribution (x-component at its maximum amplitude value) on the top broad wall of the RGW structure (without slots). (a) With grooves at 76 GHz. (b) With notches at 104 GHz.

To further illustrate the impact of grooves, a single RGW structure (with grooves but without slots) is simulated in the traveling-wave scenario (with two ports at both sides and one of the ports excited) to examine the surface electric current distribution on the top broad wall of the RGW. Fig. 4(a) shows the transverse component (x-component) of the surface electric current (at its maximum value) at 76 GHz, where a nonuniform distribution can be observed. Particularly, the transverse current on the top wall is notably weaker in the regions where grooves are located beneath. Considering the working mechanism of the longitudinal slot array that slots interrupt transverse electric currents to generate radiation, placing LF slots in these regions with weaker currents would result in decreased effective conductance (radiation intensity). Therefore, the LF slots will become less overloaded.

The groove's underloading effect can be represented by the circuit model shown in Fig. 5(a). Typically, a longitudinal slot is modeled as a shunt conductance, and the groove can be simply considered as an additional parallel conductance g_{Groove}, which is negative in this case. The total normalized conductance (g_{Total}) of the slot-groove pair can be quantified through S-parameter simulations in a two-port model [35], given by

$$g_{Total} = \mathrm{Re}\left\{-\frac{2S_{11}}{1+S_{11}}\right\}. \quad (1)$$

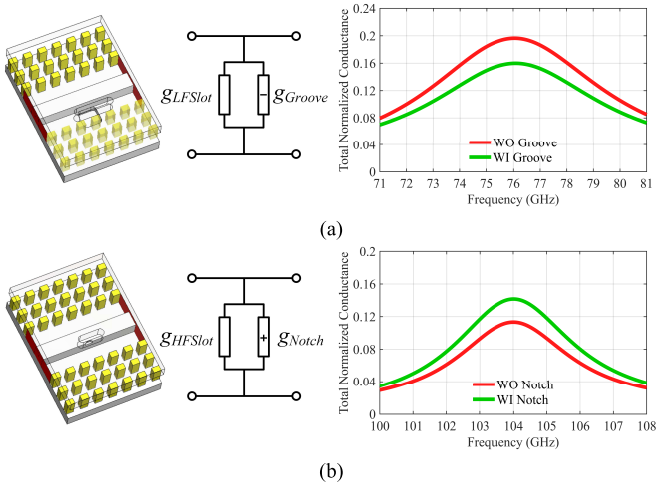

Fig. 5. Equivalent circuit models for slot geometries with integrated matching structures and their influence on normalized conductance. (a) Groove. (b) Notch.

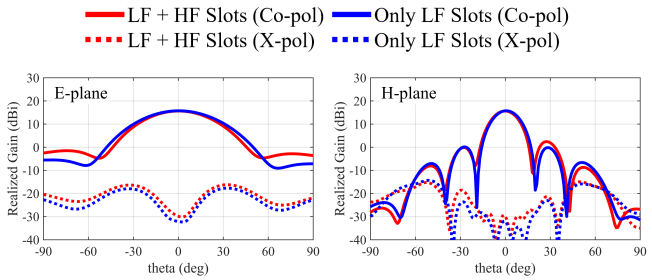

Fig. 6. Comparison of simulated radiation patterns at 76 GHz.

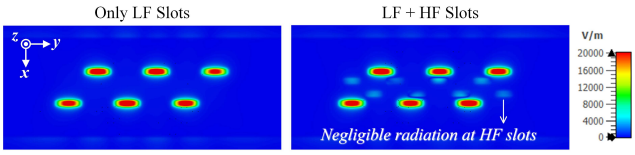

Fig. 7. Comparison of E-field distribution (x-component) at 76 GHz (0.1 mm above the aperture).

The calculated results in Fig. 5(a) clearly indicate a reduction in normalized conductance upon the implementation of the groove, which is consistent with the weaker transverse surface current in the groove region, as shown in Fig. 4(a). (Note that these conductance values are not exactly identical to those of the optimized slots in the final dual-band subarray due to structural differences.)

Furthermore, the local introduction of the groove does not alter the major dimensions of the original RGW; as a result, it only slightly detunes the dual-band slots, a situation easily remedied by fine-tuning the slot lengths. Additionally, as long as the groove size is not excessively large, it has minimal impact on the HF radiation pattern. It should be noted that an overall vertical extension of the RGW structure can also generate a similar underloading effect for LF slots. Still, it could significantly detune the HF slots and destroy the well-tuned HF S_{11} performance.

For the HF band, notches are implemented along the edges of the ridge beneath each HF slot to achieve a broader bandwidth by introducing an overloading effect. As depicted in Fig. 3, the HF −10-dB bandwidth is extended from around 3.7 to 5.7 GHz upon the deployment of notches, with two resonances lower than −15 dB on either side of the center frequency. Following the same methodology as for grooves, an RGW structure (with notches but without slots) is examined. Fig. 4(b) shows the surface electric current's transverse component (x-component) on RGW's top broad wall at 104 GHz. The transverse current becomes noticeably stronger in the regions where notches are implemented beneath, which increases the effective conductance (radiation intensity) when HF slots are deployed. Consequently, an overloading effect can be achieved.

Notably, in this simulation, some noticeable reflections from the notches can be observed near the feeding port (on the left), as shown in Fig. 4(b). However, these reflections will not exist when the radiating slots are implemented and well-tuned. Additionally, the approximately semicircular shape of the notch in the final design, as shown in Fig. 1, was adopted to accommodate CNC fabrication techniques.

The notch can similarly be represented as a positive parallel conductance g_{Notch} in the circuit model [Fig. 5(b)]. The g_{Total} of the slot–notch pair can also be calculated using (1). The calculated results demonstrate an increase in normalized conductance upon the implementation of the notch, which is consistent with the stronger transverse surface current in the notch region, as shown in Fig. 4(b).

In addition, the introduction of notches will only have a minimal effect on the resonance frequency of HF slots, which can also be easily adjusted by fine-tuning the slot length. Given that the notches are located far from the LF slots and have small electrical dimensions at the LF band, they will not influence the LF performance.

In summary, the groove and notch have opposite effects on the slot's effective conductance at their respective bands and have no significant impact on each other's bands. This enables the subarray's dual-band reflection coefficient to be improved oppositely and independently.

C. Dual-Band Radiation Patterns

In addition to the impedance matching, the radiation pattern of the dual-band subarray is also examined, particularly focusing on the mutual influence of dual-band slots.

At the LF band, using the same methodology described in Section II-A, the slot array is analyzed under two scenarios: one with only LF slots and the other with dual-band slots. As illustrated in Fig. 6, after the implementation of HF slots, the 3-dB E-plane beamwidth at 76 GHz decreases from 43.8° to 40.4°, and the gain increases from 15.7 to 15.8 dBi. This trivial difference is because the HF slots are basically cut off at the LF band, barely contributing to the LF radiation. The E-field distribution (x-component) above the aperture at 76 GHz for both cases is depicted in Fig. 7 to demonstrate this behavior. When dual-band slots are implemented, the electric field at the HF slots is very weak compared to that at the LF slots.

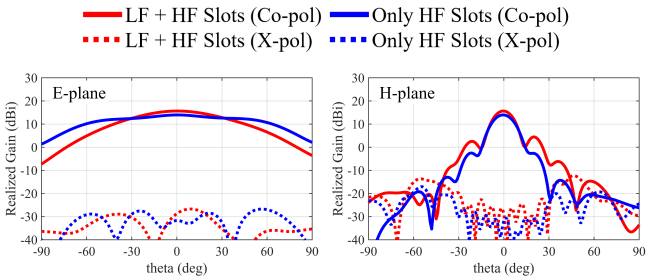

Fig. 8. Comparison of simulated radiation patterns at 104 GHz.

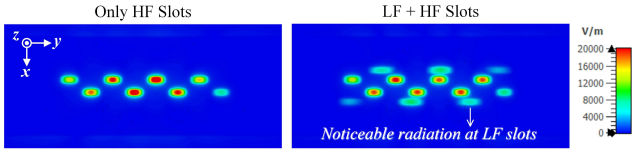

Fig. 9. Comparison of *E*-field distribution (x-component) at 104 GHz (0.1 mm above the aperture).

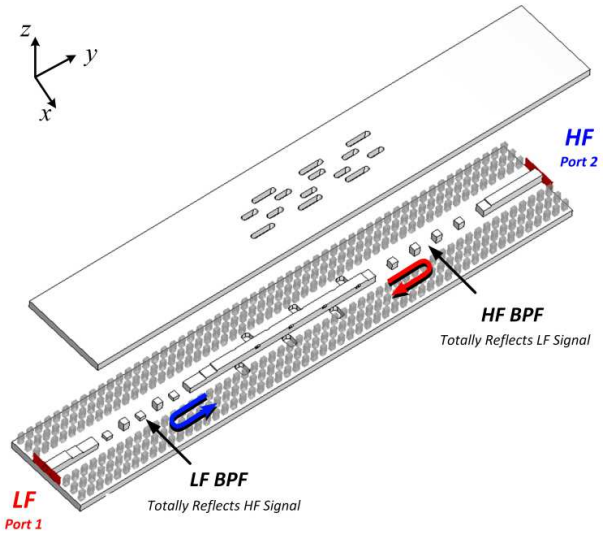

Fig. 10. Exploded view of dual-band subarray incorporated with BPFs.

Therefore, the overall radiation performance in the LF band is similar, regardless of the presence of HF slots.

Additionally, the subarray's LF E-plane pattern is inherently narrow due to the relatively wide transverse spacing (double the offset) between the LF slots, which equals 0.56 wavelength at 76 GHz (2.35 mm, as shown in Fig. 1). Fig. 6 provides a comparison of H-plane patterns, also showcasing negligible variance.

A similar comparison is conducted at the HF band, but the performance is different. As depicted in Fig. 8, in the absence of LF slots, the E-plane pattern at 104 GHz is considerably wide, with a 3-dB beamwidth of 113.2° and a gain of 13.7 dBi. This is due to the transverse spacing between HF slots being only 0.31 wavelengths at 104 GHz (0.9 mm, as shown in Fig. 1). After implementing the LF slots, the beamwidth decreases to 63.4°, and the gain increases to 15.5 dBi since the LF slots also partially contribute to the HF radiation. Fig. 9 illustrates the *E*-field distribution at 104 GHz for both cases. Noticeable radiation is observed at the LF slots, which are nearly in phase with the radiation at the HF slots. This is equivalent to increasing the radiation aperture of the subarray at the HF band. The H-plane patterns also demonstrate the gain enhancement, as depicted in Fig. 8. Although there is some degradation of the H-plane sidelobe level (SLL), it remains lower than −12 dB.

It should be noted that the higher gain and narrower beamwidth are beneficial when extending the subarray along the E-plane to form a single beam planar array. Due to the existence of dual-band slots and the manufacturing concerns at such frequencies, the width of the subarray channel reaches 1.2 wavelength at 104 GHz (3.1 mm, as shown in Fig. 1), typically introducing the risk of grating lobes. However, the HF gain enhancement from the LF slot radiation will effectively suppress the grating lobes.

Based on these simulation results, the proposed subarray can achieve a desirable performance at dual bands, demonstrating the feasibility of this dual-band slot layout and the matching techniques.

III. Dual-Band Subarray With Filter Feeding

To achieve independent feeding at both bands, a unique configuration is employed with two BPFs incorporated on either side of the subarray, as illustrated in Fig. 10. In this setup, when the subarray is excited at the LF band through the LF BPF, the HF BPF reflects all the signal received on the opposite side, provided that it effectively rejects the LF band. Similarly, this principle applies to HF excitation. As a result, the subarray functions as a standing wave slot antenna at both bands. This special filtering feeding method aligns with the inherent characteristics of the resonant slot array, and it offers an alternative to using a complex diplexer for dual-band excitation, providing greater flexibility in system integration.

A. Designs of BPFs

Figs. 11 and 12 illustrate the designs of the HF and LF BPFs, respectively. Inline groove GWG (GGW) resonant cavities coupled through coupling posts are employed [36]. The filters are fed using RGW, incorporating a GGW-to-RGW transition [29], to facilitate integration with the slot array antenna.

The detailed dimensions of the HF BPF are provided in Fig. 11. The simulated frequency response is shown in Fig. 13, demonstrating that the design specifications have been successfully met. A passband with insertion loss better than −20 dB is achieved within the HF band, while a rejection level exceeding 35 dB is observed in the LF band.

The LF BPF is designed using the same approach, and its detailed dimensions are provided in Fig. 12. The only difference is that a tuning pin is added at the center of each resonant cavity in the final design to shift the TE_{101} mode to the desired frequency range, thereby eliminating the undesired response around 100 GHz [37]. The simulated

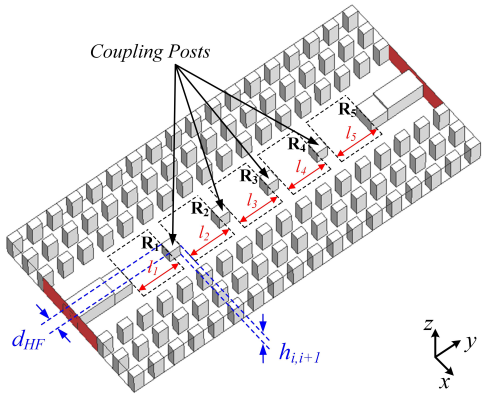

Fig. 11. Schematic view of the HF BPF with the top plate removed (R_i represents the resonant cavities, d_{HF} = 0.4 mm, h_{12} = h_{45} = 0.56 mm, h_{23} = h_{34} = 0.63 mm, l_1 = l_5 = 1.65 mm, l_2 = l_4 = 1.58 mm, and l_3 = 1.54 mm.)

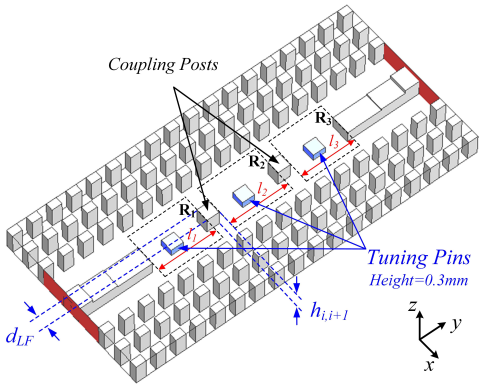

Fig. 12. Schematic view of the LF BPF with the top plate removed (R_i represents the resonant cavities, d_{LF} = 0.5 mm, h_{12} = h_{23} = 0.65 mm, l_1= l_3 = 2.30 mm, and l_2 = 3.42 mm.)

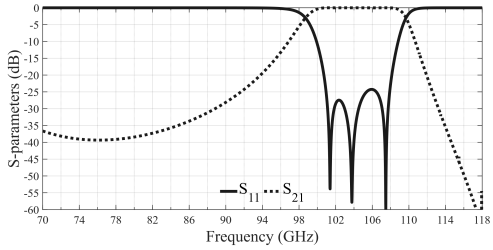

Fig. 13. Simulated frequency response of the HF BPF.

frequency response, with and without the inclusion of the pins, is presented in Fig. 14. A passband with insertion loss better than −20 dB is achieved within the LF band, while a rejection level exceeding 40 dB is obtained in the HF operating band.

B. Subarray Incorporated With BPFs

Then, as shown in Fig. 10, the HF and LF BPFs designed above are incorporated at both sides of the slot array, with proper distances from the slots to provide the desired standing wave distribution for slot excitation. Fig. 15 illustrates the simulated S-parameters of the subarray. Around 4-GHz

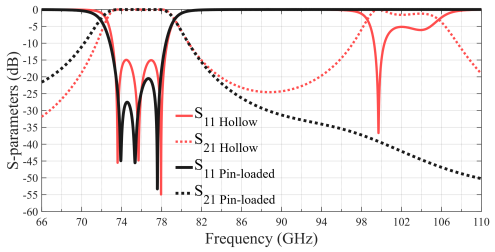

Fig. 14. Comparison of the simulated LF BPF designed with hollow and pin-loaded cavities.

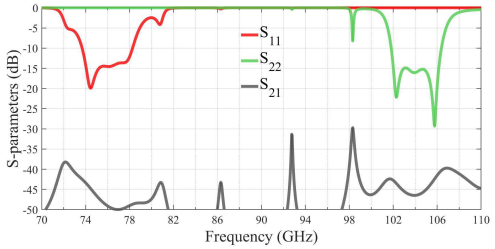

Fig. 15. Simulated S-parameters of the subarray incorporated with BPFs.

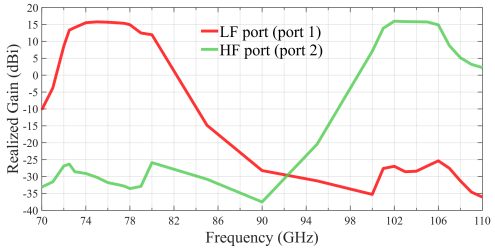

Fig. 16. Simulated realized gain of the subarray incorporated with BPFs.

bandwidths (74–78 and 102–106 GHz) are achieved at HF and LF bands. Since both BPFs provide good rejection on the other band, better than 40-dB isolation between the two feeding ports is achieved at both bands. The realized gain (Fig. 16) shows the filtering characteristics at both bands, where the LF gain is around 15.5 dBi and the HF gain is around 15.8 dBi, and quite a sharp decrease is observed at the two sides of the operating bands. The radiation pattern of the subarray is presented in Fig. 17. The H-plane SLLs are −15.2, −15.1, and −12.3 dB at 74, 76, and 78 GHz, respectively, and −11.8, −11.3, and −10.3 dB at 102, 104, and 106 GHz, respectively. The simulation results of the single-column subarray show the feasibility of the scheme.

IV. Four-Column Planar Array

The proposed subarray can be extended along the E-plane into a multicolumn planar array, potentially supporting dual-band MIMO functionality (e.g., MIMO radar) when integrated with independent feeding ports for each subarray or broadside fixed-beam radiation when fed by power dividers. Specifically, the RGW architecture effectively reduces the lateral dimension of the subarray, thereby efficiently suppressing grating lobes under broadside radiation. In this section, both cases are

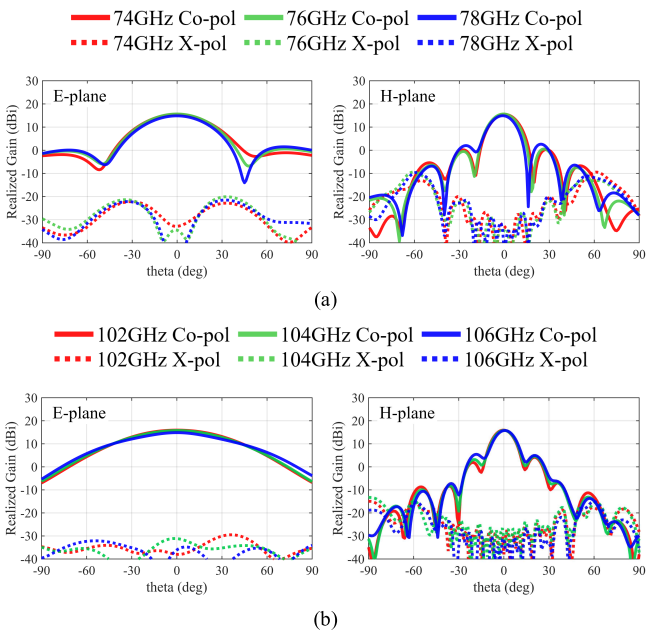

Fig. 17. Simulated radiation patterns of the subarray incorporated with BPFs. (a) LF band, 74–78 GHz. (b) HF band, 102–106 GHz.

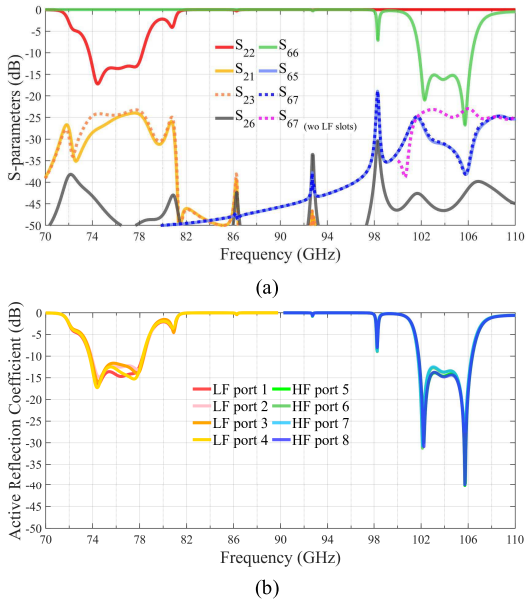

Fig. 19. (a) Simulated S-parameters of the four-column planar array with independent feeding. (b) Active reflection coefficients when all ports are simultaneously excited.

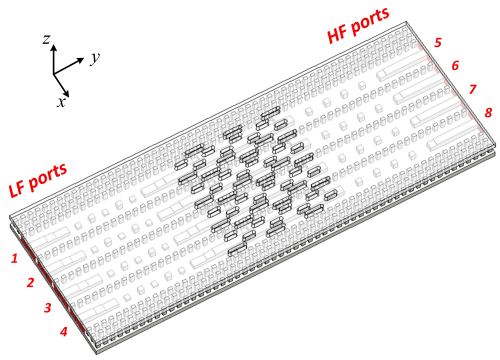

Fig. 18. Structure of the four-column planar array with independent feeding ports.

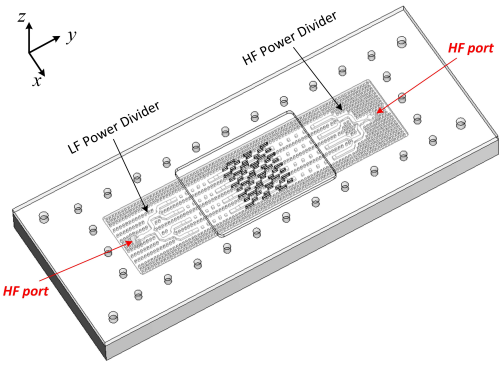

Fig. 20. Structure of the four-column planar array fed by power dividers (two ports are at the bottom).

simulated and analyzed. A fixed-beam radiation case has been chosen for manufacturing to verify the performance.

A. Four-Column Planar Array With Independent Feeding Ports for MIMO Scenario

Fig. 18 illustrates the four-column planar array with eight independent feeding ports for both bands. One row of pins is placed between adjacent columns to achieve a narrow subarray spacing. The simulated S-parameters of the center column (at Ports 2 and 6) are given in Fig. 19(a), where the reflection coefficients (S_{22} and S_{66}) and rejections (S_{26} and S_{62}) at both frequency bands are basically the same as those of the isolated subarray, as given in Fig. 15.

The mutual coupling between adjacent columns at the LF band (S_{21} and S_{23}) is quite low, below −24 dB. As shown in Fig. 19(a), although the LF slots near the interface of the two columns are in close proximity, their interleaved arrangement along the Y-axis prevents the occurrence of strong mutual coupling. The main coupling, instead, arises from the LF slots sharing the same Y-coordinate and spaced at a subarray spacing distance (3.1 mm, equivalent to 0.785 wavelengths at 76 GHz).

The mutual coupling (S_{65} and S_{67}) at the HF band is even lower, below −30 dB. This is primarily attributed to the dual-slot configuration, where the HF lateral radiation is suppressed by the LF slots, as explained in Section II (Fig. 8). For reference, S_{76} of the four-column array without LF slots is also simulated and presented in Fig. 19(a) (purple line), approximately equal to −24 dB at the HF band. This 6-dB difference suggests that LF slots also operate as a decoupling structure at the HF band in addition to a gain enhancement technique in this design. The simulated performance suggests that the proposed slot array can be a good candidate for dual-band MIMO applications.

As a supplement, the active reflection coefficients when all ports are simultaneously excited with equal amplitude and

TABLE I

GAINS, RADIATION EFFICIENCIES, AND SLLS OF THE PROTOTYPE

Frequency (GHz)	Realized Gain (dBi)			Radiation Efficiency		Measured SLL (dB)	
	Simulated with PEC	Simulated with gold (Surface roughness=0.4um)	Measured	Simulated	Measured	E-plane	H-plane
74	20.2	19.4	19.4	85%	85%	-12.9	-12.8
76	20.9	20.2	20.1	86%	85%	-14.6	-11.8
78	21.1	20.3	20.4	86%	85%	-14.3	-11.1
102	22.5	21.3	21.3	78%	78%	-14.6	-15.1
104	22.5	21.4	21.4	79%	78%	-13.7	-12.6
106	22.6	21.4	21.3	78%	78%	-12.7	-10.4

TABLE II

COMPARISON OF DUAL-BAND SLOT ARRAY SCHEMES

	Dual-Band Implementation	Polarization	Potential for Independent Channel	Dual Bands LF / HF (GHz)	Bandwidth LF / HF	Gain LF / HF (dBi)
[6]	Coaxial cavity with feeding network	S	No	20 / 30	10 % / 6.7 %	17 / 19
[7]	High-order mode cavity resonator	V H		9.87 / 10.13	0.61 % / 0.79 %	16.7 / 15.8
[9]	Interleaved WGs	V H	Yes	30 / 35	0.67 % / 1.97 %	24.8 / 25.4
[10]		V H		35 / 35	2.3 % / 2.3 %	-
[11]		V H		1.6 / 2.1	9.6 % / 12.4 %	21.5 / 22.1
[15]	Interleaved and Stacked WGs	S		16 / 35	3.13 % / 5.0 %	15.8 / 24.1
[17]		S		X / K	-	23 / 30
[19]	Shared WG (2-way radiation)	S		2.3 / 4.6	15 % / 6.5 %	12.7 / 16.4
[20]		V H		2.5 / 4.9	11.42 % / 3.27 %	11.12 / 18.92
[21]	Shared WG (distributed aperture)	S		8.6 / 10.8	0.85 % /1.25 %	7.7 / 10.8
[24]	Shared WG (corporate-fed)	V H		9.6 / 11.9	4.1 % / 5.7 %	- / 15
This work	Shared WG (shared aperture)	S		76 / 104	5.3 % / 3.9 %	20 / 21

V H = Vertical and Horizontal polarization, S = Single polarization, WG = Waveguide

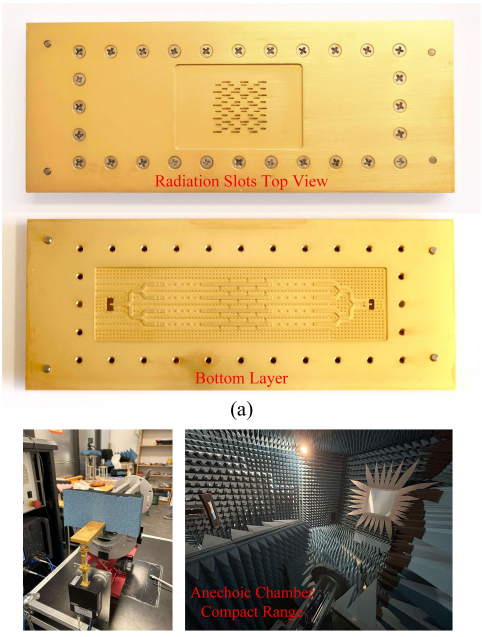

Fig. 21. (a) Manufactured prototype. (b) Measurement environment.

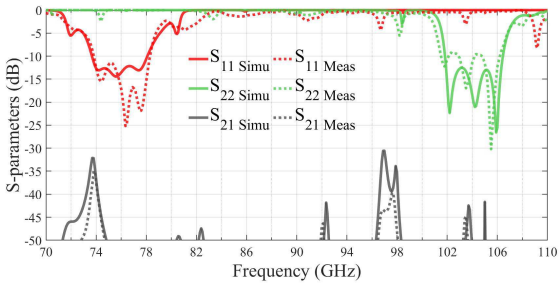

Fig. 22. Simulated and measured S-parameters of the prototype.

phase are shown in Fig. 19(b). Due to the low mutual coupling, they are similar to the reflection coefficients in Fig. 19(a).

As a supplement, the active reflection coefficients when all ports are simultaneously excited with equal amplitude and phase are shown in Fig. 19(b). Due to the low mutual coupling, they are similar to the reflection coefficients in Fig. 19(a).

B. Four-Column Planar Array Fed by Power Dividers for Fixed Beam Radiation

To achieve dual-band fixed beam radiation, two 1-to-4 power dividers are deployed on both sides of the planar array for equal-power and in-phase excitation, as shown in Fig. 20. For this fixed beam scenario, the power divider is placed between the slot array and the BPF, partly to ensure design consistency, but more importantly because the virtual short-circuit point provided by the BPF needs to be as close as possible to the slot array to avoid bandwidth reduction.

The feeding ports of the two power dividers are each transitioned to WR-10 standard waveguides for measurement. The top layer of the prototype is thickened around the radiation apertures by 1 mm to enhance structural strength, which does not impact the performance since it is relatively far from the radiation slots. In this design, filters and power dividers are

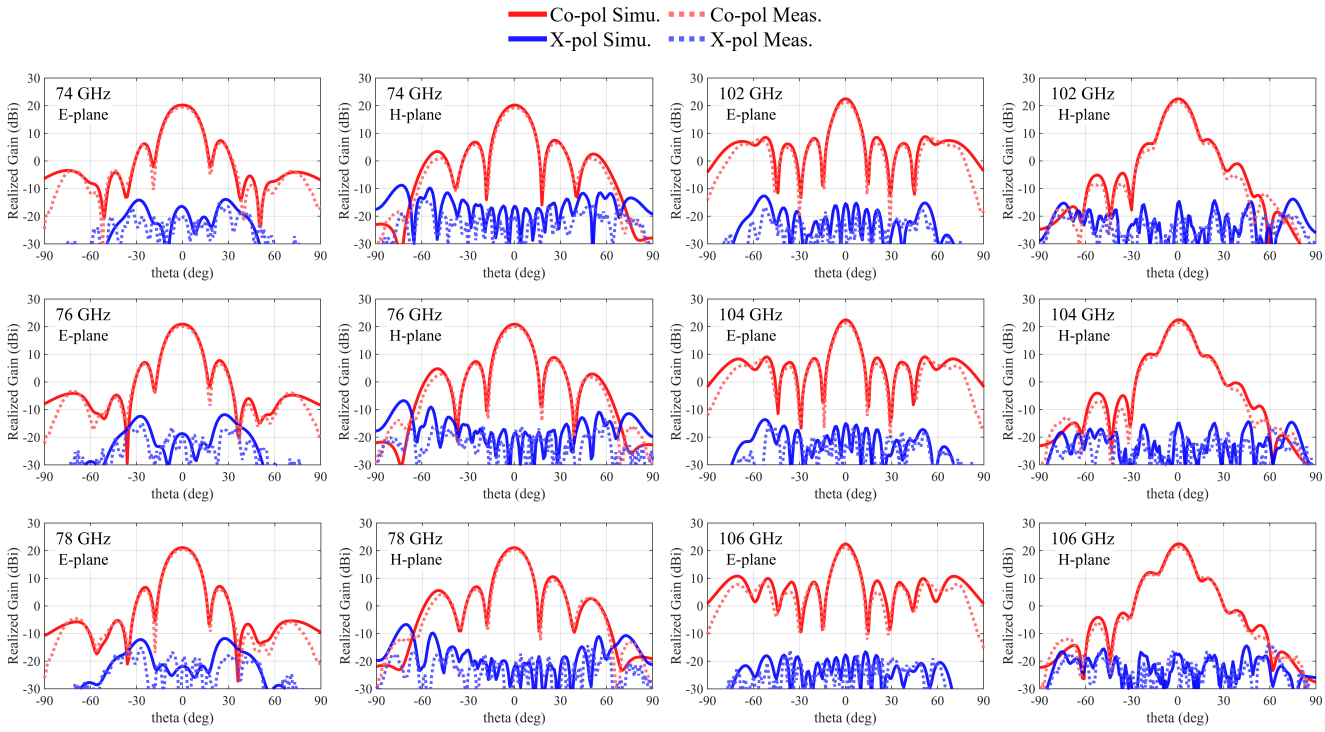

Fig. 23. Simulated and measured radiation patterns of the four-column planar array prototype.

configured at the same layer as the slot array antenna for simplicity and to prove the concept. If a smaller antenna footprint is required, it can be constructed in a multilayer architecture to minimize the overall size further. Fig. 21(a) shows the prototype, which was CNC-milled from brass and finished with gold plating, and the measurement environment is illustrated in Fig. 21(b).

Fig. 22 illustrates the simulated and measured S-parameters of the prototype. The simulated reflection coefficients at both bands are very similar to the active reflection coefficients of the four-column array [Fig. 19(b)], as the insertion losses introduced by the power dividers and transitions are negligible. The −10-dB bandwidth covers 74–78 and 102–106 GHz, respectively. The measured results match the simulation quite well despite the slight degradation in the HF band (above 100 GHz), which should be due to the manufacturing tolerances.

Fig. 23 illustrates the simulated (PEC) and measured radiation patterns. Table I lists the simulated and measured data of gains and SLLs. In addition to the simulated gain results using PEC, we have also performed simulations using gold material with surface roughness (0.4 μm) based on the fabrication process, obtaining corresponding radiation efficiencies of approximately 86% and 78% at LF and HF, respectively. By comparing the simulated and measured data, the measured efficiencies are estimated to be approximately 85% and 78%, which show good agreement with the simulations. The detailed simulated gains corresponding to these efficiencies are also provided in Table I.

The proposed work and previously reported dual-band slot arrays are compared and presented in Table II. Our design implements a GWG-based shared waveguide solution with a planar structure and aperture at the W-band, avoiding the complexity of densely packed or stacked waveguide configurations and providing filtering characteristics through integrated BPFs. This makes this work a good candidate for HF applications.

V. Conclusion

This article has presented a linearly polarized dual-band slot array antenna operating at 74–78 and 102–106 GHz, featuring shared waveguide channels for dual-band slots and a planar aperture. Two BPFs have been employed to obtain the dual-band independent feeding and filtering characteristics. The dual-band subarray has the potential to be used in MIMO and fixed-beam applications. A planar array prototype of four subarray columns has been fabricated and manufactured to verify this concept. This work has provided a new dual-band slot array solution with a simpler structure and desired performance. The broader frequency ratio range (1:1.2–1:1.85) supported by this configuration will be explored in future work.

References

[1] R. Elliott, "An improved design procedure for small arrays of shunt slots," *IEEE Trans. Antennas Propag.*, vol. AP-31, no. 1, pp. 48–53, Jan. 1983.

[2] L. Josefsson, "Analysis of longitudinal slots in rectangular waveguides," *IEEE Trans. Antennas Propag.*, vol. AP-35, no. 12, pp. 1351–1357, Dec. 1987.

[3] J. He, Y. Wu, D. Chen, M. Zhang, J. Hirokawa, and Q. Liu, "Realization of a wideband series-fed 4×4-element waveguide slot array in the X-band," *IEEE Access*, vol. 9, pp. 83666–83675, 2021.

[4] J.-L.-A. Lijarcio, A. Vosoogh, C. Bencivenni, and A. U. Zaman, "Low-cost center-fed slot array based on gap waveguide MLW coaxial line technology for E-band automotive radar," *IEEE Trans. Antennas Propag.*, vol. 72, no. 7, pp. 5674–5681, Jul. 2024.

[5] M. Fang, J. Yang, T. Emanuelsson, I. Andersson, and A. U. Zaman, "1-D wide scanning gap waveguide-based slot array antenna using decoupling technique for 100 GHz applications," *IEEE Trans. Antennas Propag.*, vol. 72, no. 4, pp. 3438–3450, Apr. 2024.

[6] M. Ferrando-Rocher, J. I. Herranz-Herruzo, A. Valero-Nogueira, and M. Baquero-Escudero, "Dual-band single-layer slot array antenna fed by K/Ka-band dual-mode resonators in gap waveguide technology," *IEEE Antennas Wireless Propag. Lett.*, vol. 20, pp. 416–420, 2021.

[7] J.-Y. Lin, Y. Yang, S.-W. Wong, and Y. Li, "High-order modes analysis and its applications to dual-band dual-polarized filtering cavity slot arrays," *IEEE Trans. Microw. Theory Techn.*, vol. 69, no. 6, pp. 3084–3092, Jun. 2021.

[8] A. G. Derneryd and A. Lagerstedt, "Novel slotted waveguide antenna with polarimetric capabilities," in *Proc. Int. Geosci. Remote Sens. Symp., Quant. Remote Sens. Sci. Appl. (IGARSS)*, vol. 3, Florence, Italy, 1995, pp. 2054–2056.

[9] T. Li, H. Meng, and W. Dou, "Design and implementation of dual-frequency dual-polarization slotted waveguide antenna array for Ka-band application," *IEEE Antennas Wireless Propag. Lett.*, vol. 13, pp. 1317–1320, 2014.

[10] Y. Cong and W. Dou, "Design of dual-polarized waveguide slotted antenna array for Ka-band application," in *Proc. 9th Int. Symp. Antennas, Propag. EM Theory*, Guangzhou, China, Nov. 2010, pp. 97–100.

[11] H. Luo, Y. Xiao, X. Lu, and H. Sun, "Design of a dual-polarization single-ridged waveguide slot array with enhanced bandwidth," *IEEE Antennas Wireless Propag. Lett.*, vol. 18, pp. 138–142, 2019.

[12] W. Wang, J. Jin, J.-G. Lu, and S.-S. Zhong, "Waveguide slotted antenna array with broadband, dual-polarization and low cross-polarization for X-band SAR applications," in *Proc. IEEE Int. Radar Conf.*, Sep. 2005, pp. 653–656.

[13] Z. Wang, Y. Wang, M. Xie, Z. Huang, and P. Chen, "Design of W-band dual polarized slotted waveguide array antenna on an annular disk," *J. Infr., Millim., THz Waves*, vol. 44, nos. 1–2, pp. 151–168, Feb. 2023.

[14] M. Chen, X.-C. Fang, W. Wang, H.-T. Zhang, and G.-L. Huang, "Dual-band dual-polarized waveguide slot antenna for SAR applications," *IEEE Antennas Wireless Propag. Lett.*, vol. 19, pp. 1719–1723, 2020.

[15] Y. Rao, H. Zhang, and G. Sun, "Shared aperture dual-band waveguide slot antenna," in *Proc. IEEE Int. Symp. Antennas Propag. North Amer. Radio Sci. Meeting*, Jul. 2020, pp. 693–694.

[16] G. Colangelo and R. Vitiello, "Shared aperture dual band printed antenna," in *Proc. Int. Conf. Electromagn. Adv. Appl.*, Sep. 2011, pp. 1092–1095.

[17] Y.-Y. Liu, F.-W. Yao, and Y.-B. Shang, "Co-aperture dualband waveguide monopulse antenna," in *Proc. Int. Symp. Antennas Propag. (ISAP)*, Apr. 2013, pp. 1–3.

[18] D.-J. Wei, J. Li, G. Yang, J. Liu, and J.-J. Yang, "Design of compact dual-band SIW slotted array antenna," *IEEE Antennas Wireless Propag. Lett.*, vol. 17, pp. 1085–1089, 2018.

[19] I. F. da Costa, D. H. Spadoti, and S. A. Cerqueira, "Dual-band slotted waveguide antenna array for communication, maritime navigation and surveillance radar," in *Proc. Int. Workshop Telecommun. (IWT)*, Jun. 2015, pp. 1–4.

[20] C. S. Arismar et al., "A novel dual-polarization and dual-band slotted waveguide antenna array for dual-use radars," in *Proc. 10th Eur. Conf. Antennas Propag. (EuCAP)*, Davos, Switzerland, Apr. 2016, pp. 1–4.

[21] S. Mukherjee, K. V. Srivastava, and A. Biswas, "Implementation of dual-frequency longitudinal slot array antenna on substrate integrated waveguide at X-band," in *Proc. Eur. Microw. Conf.*, Nuremberg, Germany, Oct. 2013, pp. 195–198.

[22] Z.-X. Zeng, W. Hong, Z. Kuai, H. Tang, and J. Chen, "The design and experiment of a dual-band omni-directional SIW slot array antenna," in *Proc. Asia Pac. Microw. Conf.*, Dec. 2007, pp. 1–4.

[23] P. Kumawat and S. Joshi, "5G dual-band slotted SIW array antenna," *J. Taibah Univ. for Sci.*, vol. 15, no. 1, pp. 321–328, Jan. 2021.

[24] J. Gao, T. Li, H. Wang, X. Lei, and K. Wang, "A compact dual-band dual-linearly polarized waveguide slot array antenna with groove at waveguide bottom," *Int. J. Microw. Wireless Technol.*, vol. 15, no. 7, pp. 1205–1211, Sep. 2023.

[25] T. S. Rappaport et al., "Wireless communications and applications above 100 GHz: Opportunities and challenges for 6G and beyond," *IEEE Access*, vol. 7, pp. 78729–78757, 2019.

[26] P.-S. Kildal, E. Alfonso, A. Valero-Nogueira, and E. Rajo-Iglesias, "Local metamaterial-based waveguides in gaps between parallel metal plates," *IEEE Antennas Wireless Propag. Lett.*, vol. 8, pp. 84–87, 2009.

[27] P.-S. Kildal, A. U. Zaman, E. Rajo-Iglesias, E. Alfonso, and A. Valero-Nogueira, "Design and experimental verification of ridge gap waveguide in bed of nails for parallel-plate mode suppression," *IET Microw., Antennas Propag.*, vol. 5, no. 3, pp. 262–270, Feb. 2011.

[28] E. Rajo-Iglesias, M. Ferrando-Rocher, and A. U. Zaman, "Gap waveguide technology for millimeter-wave antenna systems," *IEEE Commun. Mag.*, vol. 56, no. 7, pp. 14–20, Jul. 2018.

[29] A. U. Zaman and P.-S. Kildal, "Wide-band slot antenna arrays with single-layer corporate-feed network in ridge gap waveguide technology," *IEEE Trans. Antennas Propag.*, vol. 62, no. 6, pp. 2992–3001, Jun. 2014.

[30] D. Santiago, M. A. G. Laso, T. Lopetegi, and I. Arregui, "Novel design method for millimeter-wave gap waveguide low-pass filters using advanced manufacturing techniques," *IEEE Access*, vol. 11, pp. 89711–89719, 2023.

[31] S. Farjana et al., "Realizing a 140 GHz gap waveguide-based array antenna by low-cost injection molding and micromachining," *J. Infr., Millim., Terahertz Waves*, vol. 42, no. 8, pp. 893–914, Aug. 2021.

[32] D. Zarifi, A. Farahbakhsh, and A. U. Zaman, "A gap waveguide-based D-band slot array antenna with interdigital feed network," *IEEE Trans. Antennas Propag.*, vol. 71, no. 9, pp. 7124–7131, Sep. 2023.

[33] W. Tan, Y. He, H. Luo, G. Zhao, and H. Sun, "A wideband high-efficiency side-connected magnetoelectric dipole antenna array using novel feeding technology for W-band," *IEEE Trans. Antennas Propag.*, vol. 72, no. 9, pp. 7383–7388, Sep. 2024.

[34] D. Santiago, M. Fang, A. U. Zaman, M. A. G. Laso, T. Lopetegi, and I. Arregui, "W-band filtering antenna based on a slot array and stacked coupled resonators using gap waveguide technology," *IEEE Antennas Wireless Propag. Lett.*, vol. 23, no. 8, pp. 2546–2550, Aug. 2024.

[35] D. M. Pozar, *Microwave Engineering*, 4th ed., Hoboken, NJ, USA: Wiley, 2011.

[36] D. Santiago et al., "Robust design of 3D-printed W-band bandpass filters using gap waveguide technology," *J. Infr., Millim., Terahertz Waves*, vol. 44, nos. 1–2, pp. 98–109, Dec. 2022.

[37] J. Weindl, A. Prasetiadi, and T. F. Eibert, "Pin-loaded rectangular hollow-waveguide cavities for filter design with excellent suppression of spurious passbands," in *Proc. 53rd Eur. Microw. Conf. (EuMC)*, Berlin, Germany, Sep. 2023, pp. 291–294.

Mu Fang received the B.S. degree in electrical engineering, and the M.S. degree in electromagnetic field and microwave technology from Harbin Institute of Technology, Harbin, China, in 2014 and 2018, respectively. He is currently pursuing the Ph.D. degree with the Chalmers University of Technology, Gothenburg, Sweden.

From 2018 to 2020, he was an Antenna Engineer at SZ DJI Technology Company Ltd. His current research interests include gap waveguide, slot array antenna, phased array antenna.

David Santiago was born in Valencia, Spain. He received the B.Sc., M.Sc., and Ph.D. degrees in elecommunication engineering from the Electrical, Electronic and Communications Engineering Department, Public University of Navarre (UPNA), Pamplona, Spain, in 2017, 2019, and 2024, respectively.

In 2023, he joined the Division of Communications, Antennas, and Optical Networks (CAOS), Chalmers University of Technology, Gothenburg, Sweden, as a Guest Researcher. He is currently an RF Engineer with Anteral S.L., Huarte, Spain.

Jian Yang (Senior Member, IEEE) received B.S. degree in electrical engineering from Nanjing University of Science and Technology, Nanjing, China, in 1982, the M.S. degree in electrical engineering from Nanjing Research Center of Electronic Engineering, Nanjing, in 1985, and the Swedish Licentiate and Ph.D. degrees from the Chalmers University of Technology, Gothenburg, Sweden, in 1998 and 2001, respectively.

From 1985 to 1996, he was with Nanjing Research Institute of Electronics Technology, Nanjing, China, as a Senior Engineer. From 1999 to 2005, he was with the Department of Electromagnetics, Chalmers University of Technology, as a Research Engineer. During 2005 and 2006, he was with COMHAT AB as a Senior Engineer. From 2006 to 2010, he was an Assistant Professor at the Department of Signals and Systems, Chalmers University of Technology. From 2010, 2016 and 2020, he has been an Associate Professor, a Professor, and a Full Professor, respectively, at the Department of Electrical Engineering, Chalmers University of Technology. He has published more than 100 journal articles and about 200 peer reviewed conference papers. H-index: 35 and i10-index: 107. His research interests include ultra-wideband antennas and UWB feeds for reflector antennas, mmWave antennas, mmWave multilayer phased array antennas, mmWave SWE (sheet waveguide element) antennas, gap waveguide antennas, UWB radar systems, UWB antennas in near-field sensing applications, hat-fed antennas, reflector antennas, radome design, and computational electromagnetics.

Ivan Arregui (Member, IEEE) received the M.Sc. and Ph.D. degrees in telecommunication engineering from the Public University of Navarre (UPNA), Pamplona, Spain, in 2005 and 2013, respectively.

He is currently an Associate Professor with the Electrical, Electronic, and Communications Engineering Department, UPNA, where he also participates as a Researcher at the Institute of Smart Cities (ISC). He is also a Co-Founder of TAFCO Metawireless S.L., Ansoáin, Spain, a spin-off company of UPNA. His research interests include periodic structure devices for microwave, millimeter-wave, and terahertz frequency ranges, numerical techniques for inverse scattering synthesis, and the design of passive components for communication satellites.

Dr. Arregui received a grant from the Spanish Ministry of Science and Innovation and several prizes, including the Extraordinary Doctorate Prize of UPNA, the HISDESAT Prize from the Spanish Telecommunications Engineers Association (COIT/AEIT) for the Best Doctoral Dissertation in Satellite Services, and the Innovation Award from Alberto Elzaburu Foundation.

Miguel A. G. Laso (Fellow, IEEE) received the M.Sc. and Ph.D. degrees in telecommunications engineering from the Public University of Navarre (UPNA), Pamplona, Spain, in 1997 and 2002, respectively.

From 1998 to 2001, he was a Doctoral Fellow Student with the Electrical and Electronic Engineering Department, UPNA, where he was an Assistant Professor, from 2001 to 2006. From 2002 to 2003, he was a Research Fellow with the Payload Systems Division, European Space Research and Technology Centre, European Space Agency (ESTEC-ESA), Noordwijk, The Netherlands.He is currently the Head of the Microwave Components Group (MCG), UPNA. He is the Co-Founder of TAFCO Metawireless S.L., Ansoain, Spain, a spin-off company of UPNA. He has been an Associate Professor (Professor Titular), since 2006, always involved in teaching and research duties related to optical communications and microwave engineering. He has authored or co-authored dozens of journal articles and contributed to major international conferences. He has led projects with public and private regional, national, and international funding within the MCG and UPNA. He holds several international patents, some of them used by the space industry. His research interests include periodic structures, inverse scattering problems, synthesis techniques for filters and multiplexers in the microwave and millimeter-wave frequency ranges, and their applications in wireless and space communications.

Dr. Laso is a member of several professional and scientific international associations, including the Optical Society of America (OSA), the International Society for Optics and Photonics (SPIE), and the American Society for Engineering Education (ASEE). He is a member of MTT-5 Filters and the MTT-S Education Committee. He is a TPRC Member of the MTT-S International Microwave Symposium (IMS), TPC member of the European Microwave Conference (EuMC), and a reviewer for several other international conferences and journals. He received several prizes, including the Spanish National Prize to the Best Doctoral Dissertation in telecommunications from the Spanish Telecommunications Engineers Association (COIT/AEIT), in 2002, the Junior Research Award of UPNA, in 2003, and the 2005 Spanish National Prize for the Best Project in Innovation in Higher Education from the Spanish Ministry of Education and Science. He was the Co-Chair of the EuMC'18 (Madrid) and he is the Co-Chair of the Education Resources Development Subcommittee. He is the Chair of the Working Group of Standards for Microwave Filter Definitions, IEEE Standards Committee. He was an Associate Editor of IEEE TRANSACTIONS ON MICROWAVE THEORY AND TECHNIQUES, from 2019 and 2022. He is the current President of the URSI Spanish National Committee.

Thomas Emanuelsson received the Master of Science degree in electronic engineering from the Chalmers University of Technology Gothenburg, Sweden, in 1984.

He is currently holding a position as a Senior Expert in Microwave and SubTHz Technology at Ericsson AB and also a position as an Adjunct Professor at the Microwave Electronics Laboratory, Department of Microtechnology and Nanoscience (MC2), Chalmers University of Technology. Extensive background in mmWave radio communication, radar phased array systems, and MMIC technology.

Ashraf Uz Zaman (Senior Member, IEEE) was born in Chittagong, Bangladesh. He received the M.Sc. and Ph.D. degrees from the Chalmers University of Technology, Gothenburg, Sweden, in 2007 and 2013, respectively.

He is currently an Associate Professor with the Communication and Antenna Systems Division, Chalmers University of Technology. His current research interests include high gain millimeter-wave planar antennas, gap waveguide technology, frequency-selective surfaces, microwave passive components, RF packaging techniques, and low-loss integration of electronics with multi-layer antenna technology.

Dr. Zaman is a member of the IEEE Microwave Theory and Techniques Society (MTT-S), the IEEE Antennas and Propagation Society (AP-S), and a reviewer of various IEEE and IET conferences and journals. He is also co-founder of the Chalmers startup company named Gapwaves AB and holds several patents.

Ahmed A. Kishk (Life Fellow, IEEE), photograph and biography not available at the time of publication.